Research Article

INDONESIAN SCHOLAR SOCIETY

Indones. J. Chem. Stud.
2026, 5(2), 90-99
Available online at journal.solusiriset.com
e-ISSN: 2830-7658; p-ISSN: 2830-778X

Indonesian Journal of Chemical Studies

Synthesis and Microwave Absorption Performance of Fe_3O_4/Graphene Nanoplatelet/Carbonized Rice Husk Nanocomposite Epoxy Coatings on Aluminum Substrates for X-Band Radar Absorption

Hendrik Indrawan Aritonang[1], Andri Hardiansyah[2], M. Zuhnir Pilliang[1], Sovian Aritonang[1], Ridho Hotmartua Manurung[1], Krisman Hans Tunggul Purba[1], Riri Murniati[1]*

[1]*Department of Physics, The Republic of Indonesia Defense University, Bogor 16810, Indonesia*

[2]*Research Center for Nanotechnology Systems, National Research and Innovation Agency (BRIN), Banten 15314, Indonesia*

Received: 27 Jun 2026; Revised: 13 Sep 2026; Accepted: 22 Sep 2026;
Published online: 12 Nov 2026; Published regularly: 31 Dec 2026

Abstract—In this study, an Fe_3O_4/graphene nanoplatelet/carbonized rice husk (Fe_3O_4/GNPs/CRH) nanocomposite was synthesized via in situ co-precipitation and used as an epoxy coating on an aluminum substrate. The carbonization of rice husk (CRH) was performed by heating the husk at 800 °C for 2 h under a continuous N_2 atmosphere. FTIR spectroscopy was used to identify the characteristic functional groups of Fe_3O_4, GNPs, CRH, and the resulting nanocomposite. The coating thickness and surface wettability were evaluated through cross-sectional thickness measurements and water contact angle measurements, respectively. Microwave absorption performance was evaluated using a vector network analyzer (VNA) in the X-band frequency range of 8–12 GHz. The Fe_3O_4/GNPs/CRH nanocomposite exhibited a maximum reflection loss (RL) of −31.88 dB at 8.60 GHz with a thickness of 3 mm and a through power of 99.93%, whereas Fe_3O_4, GNPs, and CRH exhibited maximum RL values of −23.56, −23.95, and −24.75 dB, respectively. For the epoxy coating on aluminum, the thickness increased from 0.311 to 2.066 mm as the number of coating cycles increased. The microwave absorption performance improved with increasing coating thickness, reaching a maximum RL of −27.92 dB at 8.68 GHz for a coating thickness of 2.066 mm, with a through power of 99.83%. Water contact angle measurements showed hydrophilic behavior for all coated samples, with contact angles ranging from 51.43° to 59.49°, compared with 75.38° for uncoated aluminum.

Keywords—*Carbonized rice husk; Fe_3O_4; Graphene nanoplatelets; Microwave absorption; X-band.*

1. INTRODUCTION

The advancement of radar technologies has substantially increased the demand for materials that absorb electromagnetic waves while minimizing the radar cross-section (RCS) of various objects. Radar systems, which operate through the transmission of electromagnetic pulses and the detection of the returning signals, enable the precise determination of the location, distance, and movement of targets [1]. As radar detection continues to advance, the design of effective stealth technologies has become critical, particularly in the defense and aerospace sectors. Among the various stealth approaches, radar-absorbing materials (RAMs) have attracted considerable research interest owing to their ability to attenuate incident electromagnetic radiation and suppress reflected signals. RAMs dissipate electromagnetic energy as heat through mechanisms such as interfacial polarization, dipole relaxation, conduction loss, and magnetic loss, and thus play an essential role in passive countermeasure systems [2,3].

The microwave absorption efficiency of RAMs is strongly governed by the synergistic effect of a material's dielectric and magnetic characteristics. These materials are deployed on target surfaces to absorb incident radar waves, thereby diminishing the energy reflected back toward the radar source [4]. Among various candidate materials, carbon-based composites have attracted widespread attention in RAM fabrication [5]. Among them, graphene has emerged as a promising microwave absorber due to its high dielectric loss capacity and lightweight nature [6]. Graphene nanoplatelets (GNPs), a multilayer graphene derivative, exhibit excellent electrical conductivity, high aspect ratio, and layered structures that promote conductive loss and interfacial polarization [7]. Nevertheless, the excessively high dielectric constant of pristine GNPs often leads to impedance mismatching, causing a substantial proportion of incident electromagnetic waves to be reflected rather than absorbed [8].

***Corresponding author**.
Email address: ririmurniati90@gmail.com
DOI: 10.55749/ijcs.v5i2.192

To overcome this limitation, GNPs are commonly combined with complementary materials that possess magnetic or dielectric properties. In one notable study, Zhang et al. [9] developed GNP/ZnO composites and reported a reflection loss of −44.8 dB with an effective absorption bandwidth of 4.65 GHz. In a comparable investigation, Gita et al. [10] fabricated a TiO_2/GNP composite via planetary ball milling, yielding an RL of −30.72 dB at 8.42 GHz. Collectively, these findings confirm that GNPs function as a highly effective dielectric constituent in microwave-absorbing systems when synergistically integrated with complementary functional phases.

Magnetite (Fe_3O_4) is a ferrimagnetic material that has attracted significant interest as a magnetic loss component in RAM systems. In addition to its low cost, environmental friendliness, and low toxicity, Fe_3O_4 provides magnetic loss mechanisms that complement the dielectric behavior of carbon-based materials [11]. Previous studies have reported excellent microwave absorption performance for Fe_3O_4-based carbon composites. For instance, Li et al. [12] prepared Fe_3O_4/rGO composites using an ultrasonication method, attaining a peak RL of −39 dB at 11.6 GHz at a thickness of 2.8 mm. Subsequently, Li et al. [13] extended this approach by fabricating rGO/Fe_3O_4@SiO_2 composites, which exhibited an RL of −48.34 dB with an effective absorption bandwidth of 4.88 GHz at a thickness of 2 mm. These results demonstrate the advantage of combining Fe_3O_4 with a carbon-based matrix to simultaneously utilize both dielectric and magnetic attenuation mechanisms.

In recent years, biomass-derived porous carbons have emerged as sustainable alternatives for microwave absorption applications. Their abundance, low cost, environmental compatibility, and porous structures make them attractive candidates for electromagnetic wave attenuation [14]. Rice husk, an abundant agricultural by-product rich in carbon, has received considerable attention as a precursor for functional carbon materials [15]. Yahaya et al. [16] demonstrated that rice husk ash achieved an RL of −22.7 dB in the 8.2–12.0 GHz frequency range. Carbonized rice husk (CRH), produced through controlled thermal carbonization, is a biomass-derived porous carbon material with heterogeneous phases that promote interfacial polarization, thereby enhancing electromagnetic wave absorption performance [17]. Nevertheless, studies integrating CRH with both graphene-based and magnetic components remain limited. Although considerable progress has been achieved in developing Fe_3O_4/carbon-based microwave absorbers, most previous studies have focused on binary systems, such as Fe_3O_4/graphene or Fe_3O_4/reduced graphene oxide composites. Meanwhile, the use of biomass-derived carbon, particularly carbonized rice husk (CRH), in combination with graphene nanoplatelets and magnetic nanoparticles, remains underexplored. Furthermore, limited attention has been paid to the practical implementation of such hybrid absorbers as coating systems deposited on metallic substrates used in aerospace structures. Therefore, integrating Fe_3O_4, GNPs, and CRH into an epoxy-based coating may enhance microwave absorption by harnessing the combined properties of these components, while maintaining the lightweight and durable characteristics required for radar-absorbing material applications.

Electromagnetic wave absorption coatings, which consist of a matrix and electromagnetic wave absorbers, exhibit excellent performance in practical applications [18]. Therefore, integrating Fe_3O_4, GNPs, and CRH into a coating matrix is an attractive strategy for developing lightweight, high-performance RAMs. Aluminum was selected as the substrate due to its lightweight, outstanding mechanical characteristics, and superior resistance to corrosion, rendering it a preferred material in aerospace engineering [19]. To ensure coating adhesion and durability, an epoxy matrix was employed due to its superior corrosion resistance, high electrical resistivity, and ease of processing [20]. Previous studies have demonstrated the effectiveness of epoxy-based RAM composites. Barik et al. [21] fabricated an epoxy-based composite that demonstrated a peak RL of −34.32 dB with an effective absorption bandwidth of 4.2 GHz at a 3 mm thickness. Likewise, Barik and Nath [22] obtained an RL of −33.5 dB employing an epoxy hybrid composite synthesized via ultrasonic-assisted blending, confirming the appropriateness of epoxy as a binding matrix for microwave absorbing coating systems.

Based on these considerations, the combination of Fe_3O_4, GNPs, and CRH within an epoxy coating is expected to generate synergistic effects through the coexistence of magnetic loss, conductive loss, dipolar relaxation, and interfacial polarization mechanisms, thereby improving impedance matching and electromagnetic energy dissipation.

The Fe_3O_4/GNP/CRH nanocomposite was synthesized via an in situ co-precipitation method and evaluated for use as a radar-absorbing material (RAM). The use of an in situ co-precipitation approach enables the formation of Fe_3O_4 in the presence of GNPs and CRH during composite preparation. The novelty of this study lies in the application of the Fe_3O_4/GNP/CRH nanocomposite as an epoxy coating on an aluminum substrate, a topic that has received limited attention in previous studies. The coating thickness and water contact angle were characterized using a Dino-Lite digital microscope, while the microwave absorption properties were evaluated using a vector network analyzer (VNA) in the X-band frequency range (8–12 GHz). The absorption characteristics were investigated at different thicknesses for both powder samples and epoxy-coated aluminum substrates to determine the thickness-dependent microwave absorption performance of the material.

2. EXPERIMENTAL SECTION

2.1. Materials

The materials used in this research were iron(III) chloride hexahydrate ($FeCl_3 \cdot 6H_2O$) and iron(II) sulfate heptahydrate ($FeSO_4 \cdot 7H_2O$), which were utilized as precursor compounds for Fe_3O_4 preparation, with an aqueous ammonia solution (NH_3 25%) serving as the precipitating reagent. Graphene nanoplatelets (GNPs) were used as a constituent material of the nanocomposite, while Carbonized Rice Husk (CRH) was prepared independently through a thermal carbonization process from raw rice husk. Aluminum substrates were used as the deposition medium for the coating, while epoxy was employed as the binding matrix. The chemical reagents $FeCl_3 \cdot 6H_2O$, $FeSO_4 \cdot 7H_2O$, NH_3, and GNPs were all sourced from Sigma-Aldrich and used as received, without further purification.

2.2. Instrumentation

The coating thickness and water contact angle were measured using a Dino-Lite Digital Microscope (model AM3113T), manufactured in Taiwan. The functional group analysis was performed by BARCOV BRQ-208 FTIR. The microwave absorption properties were assessed using a Vector Network Analyzer (VNA), specifically the Anritsu MS2038C model manufactured in Japan. Data were analyzed using Origin 2021 software.

2.3. Preparation of Carbonized Rice Husk (CRH)

The preparation of CRH is shown in **Fig. 1.** Rice husk was thermally carbonized. Raw rice husk was initially cleaned with distilled water to remove surface impurities, then dried in an oven at 105°C for 24 hours before being carbonized in a tube furnace at 800°C for 2 hours under a continuous nitrogen (N_2) gas flow to prevent oxidation. After carbonization was finished, the sample was left to cool naturally to room temperature. It was then crushed with a mortar and pestle and passed through a 400-mesh sieve to produce micrometer-sized carbonized rice husk (CRH) powder.

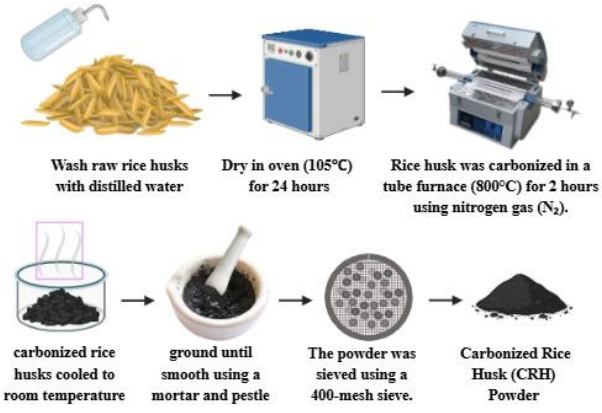


Fig. 1 Schematic of CRH preparation via thermal carbonization

2.4. Preparation of Nanocomposite

The Fe_3O_4/GNPs/CRH nanocomposite was synthesized through an in situ co-precipitation approach (**Fig. 2**) by dissolving 5.2 g of $FeCl_3 \cdot 6H_2O$ and 2.8 g of $FeSO_4 \cdot 7H_2O$ in 100 mL of deionized water. Subsequently, 1 g of GNPs and 1 g of CRH were introduced into the solution and stirred until a homogeneous mixture was obtained. This mixture was then heated to 60°C, followed by the dropwise addition of 20 mL of ammonia solution (NH_3 25%) while stirring at 150 rpm for 5 minutes. The resulting precipitate was collected using a neodymium (NdFeB) magnet, rinsed with ethanol and deionized water until a neutral pH was reached, and subsequently dried in an oven at 60°C for 24 h.

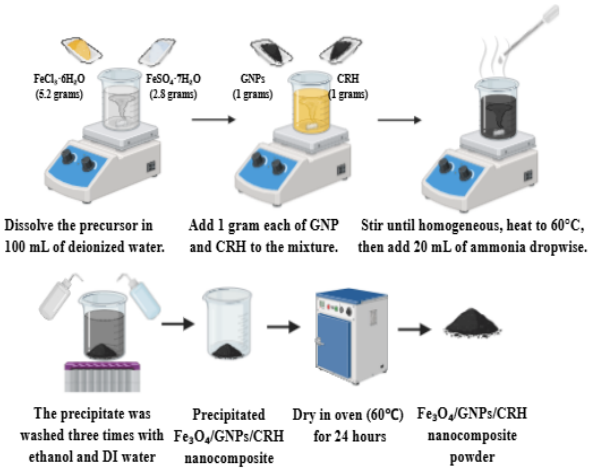


Fig. 2 Schematic of the coprecipitation synthesis method for Fe_3O_4/GNP/CRH nanocomposites

2.5. Coating Preparation

The process of coating Fe_3O_4/GNPs/CRH nanocomposites onto aluminum substrates begins with laser-cutting the aluminum plate. Next, 1 g of Fe_3O_4/GNPs/CRH nanocomposite powder was mixed

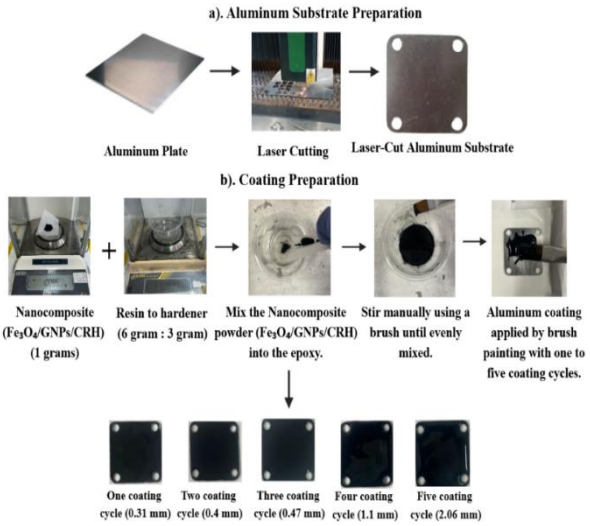


Fig. 3 Schematic illustration of (a) aluminum substrate preparation and (b) Fe_3O_4/GNPs/CRH nanocomposite coating process.

with epoxy resin and hardener at a mass ratio of 6:3, then manually stirred with a brush until homogeneous. The resulting coating mixture is applied to the aluminum substrate surface by brush painting over 1 to 5 brushing cycles, yielding layer thicknesses (in mm) of 0.31, 0.40, 0.47, 1.10, and 2.06, respectively. The process is presented in **Fig. 3.**

2.6. Thickness and Water Contact Angle

Coating thickness and water contact angle were characterized using a Dino-Lite Digital Microscope. Water contact angle analysis was performed to evaluate the surface wettability of the epoxy/Fe_3O_4/GNPs/CRH coating and assess changes in surface characteristics as coating thickness increased. This analysis provides additional information on the surface properties of the coating applied to the aluminum substrate. Coating thickness measurements were performed using cross-sectional imaging at a magnification of 26.0× with a 2.0 mm scale bar, with three measurement points taken evenly along the cross-section of the coating to obtain the average thickness. Water contact angle measurements were conducted at a magnification of 26.0× using the static sessile drop technique, with the angle measured three times at different points and averaged in DinoCapture 2.0 software. All images were recorded at a resolution of 640 × 480 pixels in MJPG format.

2.7. Microwave Absorption Performance

The Fe_3O_4/GNPs/CRH nanocomposite was characterized using a Vector Network Analyzer (VNA) over the X-band frequency range (8–12 GHz) in two sample configurations: powder samples with thicknesses of 2–5 mm and epoxy-coated aluminum substrates with coating thicknesses of 0.31, 0.40, 0.47, 1.10, and 2.06 mm. The reflection loss (RL) was determined from the S11 parameter using the Nicolson–Ross–Weir (NRW) algorithm [23]. The reflection loss (RL) represents the material's ability to absorb microwave radiation. Based on transmission line theory, the reflection loss (RL) profile of the Fe_3O_4/GNPs/CRH nanocomposite was calculated from the material's permittivity and permeability at a given frequency and sample thickness. The corresponding relationships are presented in **Eq. (1)** and **Eq. (2)** [24, 25].

$$Z_{in} = Z_0(\mu_r/\varepsilon_r)^{1/2} \tanh [j(2\pi f d/c)(\mu_r\varepsilon_r)^{1/2}] \quad (1)$$

$$RL = 20 \log | (Z_{in} - Z_0)/(Z_{in} + Z_0) | \quad (2)$$

In this context, Zin denotes the input impedance of the absorber, while Z_0 refers to the impedance of free space; μr and εr represent the relative complex permeability and permittivity, respectively, whereas f, d, and c indicate the frequency, thickness of the absorber, and speed of light, in that order. Using the previously obtained Reflection Loss (RL) values, the through power can be determined by applying **Eq. (3)** and **(4).**

$$|\tau| = 10^{RL/20} \quad (3)$$

$$Through\ power\ (\%) = (1 - \tau) \times 100\% \quad (4)$$

3. RESULTS AND DISCUSSION

3.1. Formation of CRH & Fe_3O_4/GNPs/CRH

CRH was obtained through thermal carbonization of rice husk at 800 °C for 2 h under a continuous N_2 atmosphere. During this process, the lignocellulosic components of the rice husk underwent thermal decomposition, resulting in a carbon-rich residue. The use of an inert N_2 atmosphere minimized oxidation during the carbonization process. Previous research by Mesa et al. [26] reported that rice-husk-derived carbonaceous materials obtained under controlled pyrolysis conditions contain carbonaceous structures together with oxygen-containing groups. In the present study, the resulting CRH was further characterized using FTIR.

The Fe_3O_4/GNPs/CRH nanocomposite was formed through an in situ co-precipitation process. In this process, the iron precursors were precipitated in the presence of GNPs and CRH, allowing Fe_3O_4 to form during the composite preparation. A similar approach involving the formation of Fe_3O_4 in the presence of carbon-based materials has been reported by Yang et al. [27]. The functional groups associated with the constituent materials and the changes observed after composite formation were further evaluated by FTIR.

Fig. 4 illustrates the proposed formation process of the Fe_3O_4/GNPs/CRH nanocomposite through the in-situ co-precipitation method. Initially, the Fe^{3+} and Fe^{2+} precursor solutions were mixed with GNPs and CRH. The addition of NH_3 subsequently induced precipitation of the iron species in the presence of the carbon-based components. Under these synthesis conditions, Fe_3O_4 was formed during the precipitation process, resulting in a composite containing Fe_3O_4, GNPs, and CRH. The schematic represents the sequence of the synthesis process rather than direct evidence of particle morphology or interfacial structure.

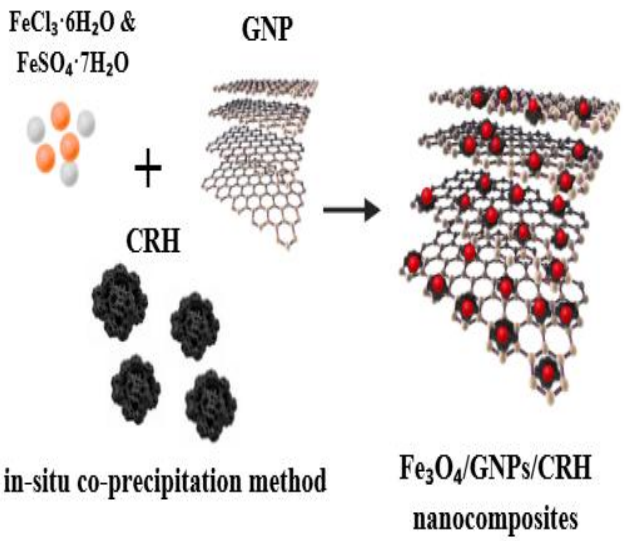


Fig. 4 Schematic formation mechanism of Fe_3O_4/GNPs/CRH Nanocomposites

3.2. FTIR Analysis

Structural FTIR analysis was performed to identify the functional groups of Fe_3O_4, GNPs, CRH, and the Fe_3O_4/GNPs/CRH composite over the wavenumber range of 4000–500 cm^{-1}, as shown in **Fig. 5**. The Fe_3O_4 spectrum shows a band at 3194 cm^{-1} associated with the O–H stretching vibration of hydroxyl groups or adsorbed water molecules on the particle surface. The band at 550 cm^{-1} corresponds to the Fe–O stretching vibration, which is characteristic of the spinel structure of Fe_3O_4 [28]. In the GNPs spectrum, the band at 3675 cm^{-1} is attributed to the O–H stretching vibration, while the band at 1642 cm^{-1} is associated with the C=C skeletal vibration of the graphitic structure [29]. The CRH spectrum shows a band at 1567 cm^{-1} associated with C=C vibration. In addition, the bands at 1025 and 778 cm^{-1} are attributed to Si–O–Si stretching and Si–O bending vibrations, respectively, indicating the presence of silica-related groups in CRH [30, 31].

In the Fe_3O_4/GNPs/CRH composite spectrum, several characteristic bands show shifts in position, as summarized in **Table 1**. The O–H bands observed in Fe_3O_4 and GNPs at 3194 and 3675 cm^{-1}, respectively, shift to 3748 cm^{-1} in the composite. This shift indicates a change in the vibrational environment of the O–H groups after composite formation. The C=C bands observed in GNPs and CRH at 1642 and 1567 cm^{-1}, respectively, shift to 1612 cm^{-1} in the composite. This shift indicates a change in the vibrational environment of the carbon structures after the three components were combined.

The Si–O–Si band of CRH at 1025 cm^{-1} shifts to 1004 cm^{-1} in the composite, while the Fe–O band of Fe_3O_4 shifts from 550 to 527 cm^{-1}. These shifts indicate changes in the vibrational environments of the Si–O–Si and Fe–O

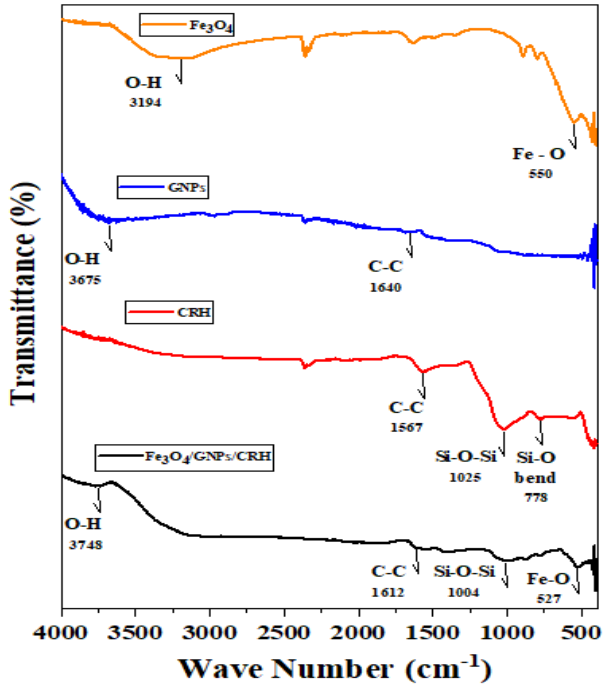


Fig. 5 FTIR spectra of Fe_3O_4, GNPs, CRH and Fe_3O_4/GNPs/CRH

Table 1. Shift in the wavenumber of the functional groups in FTIR spectra

Func. Group	Fe_3O_4 (cm^{-1})	GNPs (cm^{-1})	CRH (cm^{-1})	Fe_3O_4/GNPs/CRH (cm^{-1})
O-H	3193	3675	-	3748
C-C	-	1640	1567	1612
Si-O-Si	-	-	1025	1004
Si-O-bend	-	-	778	-
Fe-O	550	-	-	527

groups following composite formation. The Si–O bending band at 778 cm^{-1} observed in CRH is no longer clearly detected in the composite spectrum. This change may be associated with a decrease in band intensity or a change in the vibrational environment after composite formation. Overall, the characteristic bands associated with Fe_3O_4, GNPs, and CRH remain observable in the composite spectrum, although several bands exhibit shifts in position, as summarized in **Table 1**. These FTIR results support the presence of characteristic functional groups associated with the three constituent materials in the Fe_3O_4/GNPs/CRH composite.

3.3. Coating Thickness and Water Contact Angle

The coating thickness measurement results and cross-sectional observations are shown in **Fig. 6**, while the corresponding measurement data are presented in **Table 2**. Samples Al1, Al2, Al3, Al4, and Al5 represent coatings applied in 1, 2, 3, 4, and 5 coating cycles, respectively, on aluminum substrates. Based on **Fig. 6(a–e)**, the thickness of the Al/Epoxy/Fe_3O_4/GNPs/CRH coating increased with the number of coating cycles. As presented in Table 3, the average thickness values of Al1, Al2, Al3, Al4, and Al5 were 0.311, 0.403, 0.470, 1.100, and 2.066 mm, respectively.

The relationship between the number of coating cycles and the average coating thickness is shown in **Fig. 7**. The coating thickness increased gradually from Al1 to Al3, with a larger increase for Al4 and Al5. This variation indicates that increasing the number of coating cycles resulted in a thicker coating layer. The standard deviation

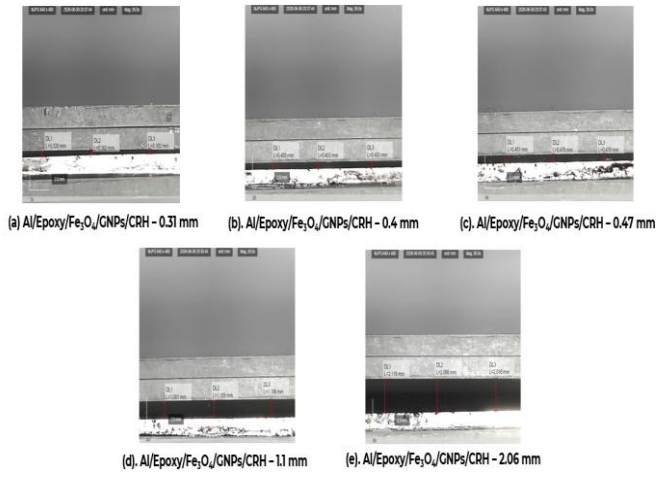


Fig. 6 Cross-sectional coating thickness of Al/Epoxy/Fe_3O_4/GNPs/CRH with thickness (a) 0.31, (b) 0.4, (c) 0.47, (d) 1.1, and (e) 2.06 mm

Table 2. Thickness data of Al/Epoxy/Fe_3O_4/GNPs/CRH from optical microscope experiments

Expe-riment	Thickness (mm)				
	Al1	Al2	Al3	Al4	Al5
1	0.328	0.403	0.453	1.083	2.116
2	0.302	0.403	0.479	1.109	2.066
3	0.302	0.403	0.479	1.109	2.016
Average	0.311	0.403	0.470	1.100	2.066
St. Dev.	0.015	0	0.015	0.015	0.050

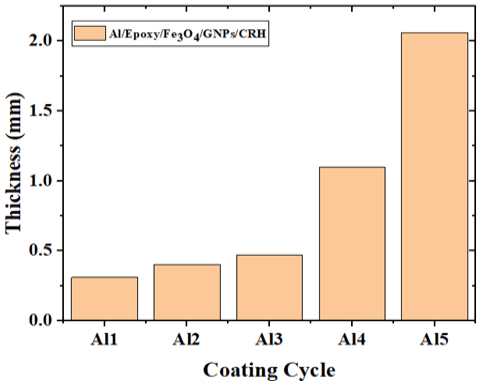


Fig. 7 Diagram of sample variation against layer thickness

values obtained from the three measurement points were 0.015, 0, 0.015, 0.015, and 0.050 mm for Al1–Al5, respectively, as shown in **Table 2**.

The cross-sectional measurements are important for determining the actual coating thickness for each coating cycle before evaluating microwave absorption performance. Since the propagation of electromagnetic waves within an absorbing layer depends on the material's thickness, accurate thickness measurements are necessary to relate the coating geometry to the reflection-loss results presented in Section 3.4. Therefore, the measured thicknesses were used to compare the microwave absorption performance of the different coating configurations.

The results of the water contact angle measurements are shown in **Fig. 8**, and the corresponding average values are given in **Table 3**. A surface is classified as hydrophilic if its contact angle falls below 90°, whereas it is considered hydrophobic when the value surpasses 90° [32].

Bare aluminum exhibited an average contact angle of 75.381°. After being coated with Epoxy/Fe_3O_4/GNPs/CRH, the contact angle decreased to 59.494°, 56.649°, 53.609°, 52.203°, and 51.434° for samples Al1 through Al5, respectively. The consistent decrease in contact angle with increasing coating thickness, as shown in **Fig. 9**, indicates a change in the surface wettability of the coated samples. This behavior is consistent with previous studies reporting that changes in the composition and surface characteristics of epoxy-based composite coatings can affect their water contact angle [33]. The presence of oxygen-containing functional groups in carbon-based materials has also been reported to influence their interaction with water molecules [34]. All samples exhibited contact angles below 90°, indicating that all surfaces, both before and after coating, are hydrophilic in nature [35].

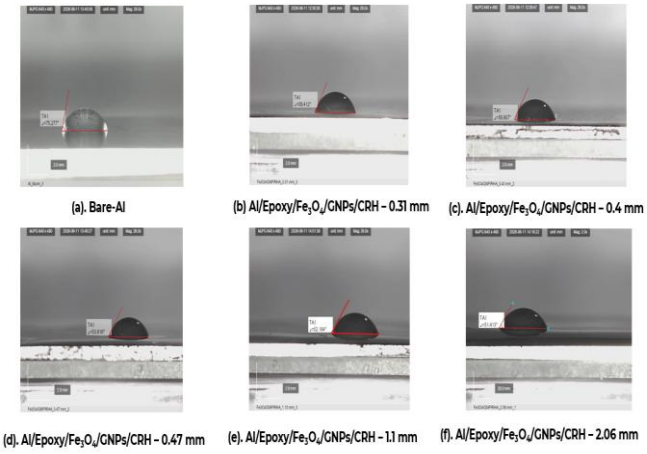


Fig. 8 Water contact angle measurement of (a) Bare-Al, Al/Epoxy/Fe_3O_4/GNPs/CRH (b) 0.31, (c) 0.4, (d) 0.47, (e) 1.1, and (f) 2.06 mm

Table 3. Contact angle data of Al/Epoxy/Fe_3O_4/GNPs/CRH from optical microscope experiments

Expe-riment	Contact Angle(°)					
	Bare-Al	Al1	Al2	Al3	Al4	Al5
1	75.967	59.273	56.409	53.336	52.319	51.413
2	74.898	59.798	56.687	53.616	52.125	51.533
3	75.277	59.412	56.850	53.874	52.164	51.356
Ave-rage	75.381	59.494	56.649	53.609	52.203	51.434
St. Dev	0.542	0.272	0.223	0.269	0.103	0.090

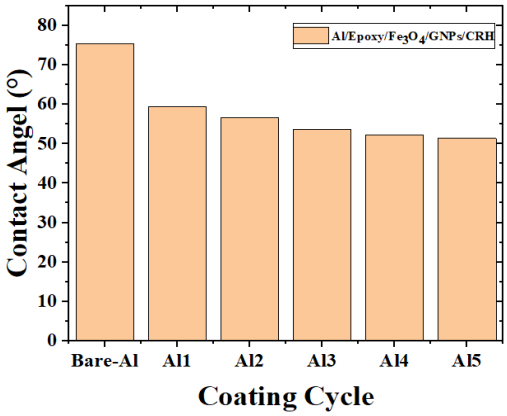


Fig. 9 Diagram of sample variation on water contact angle results

The relationship between coating thickness and water contact angle is presented in **Fig. 10**. The average contact angle decreased from 59.494° for Al1 to 51.434° for Al5 as the coating thickness increased from 0.311 to 2.066 mm. This trend shows a progressive change in the surface wettability of the coated aluminum as coating thickness increases.

Hydrophilic surfaces facilitate water spreading and generally increase the potential risk of corrosion in humid environments, as water can more readily make broad

contact with the surface [36]. Nevertheless, hydrophilicity does not necessarily eliminate a coating's protective function. The epoxy layer used as the coating matrix continues to serve as a physical barrier, restricting direct contact between water/electrolyte and the aluminum substrate, as demonstrated in neat epoxy systems that still provide significant protection despite not being hydrophobic [37]. Therefore, the Epoxy/Fe_3O_4/GNPs/CRH coating is expected to continue protecting the aluminum substrate compared with bare aluminum.

3.4. Microwave Absorbing Performance

As shown in **Fig. 10(a-c)** and **Table 4**, all three single-component materials exhibited microwave-absorbing capability within the X-band frequency range. Fe_3O_4 achieved the best reflection loss of −23.56 dB at 8.6 GHz with a thickness of 5 mm and a through power of 99.55%. The absorption in Fe_3O_4 is generally attributed to magnetic loss arising from its ferrimagnetic properties, which promote the conversion of electromagnetic energy into heat [38]. GNPs exhibited the best reflection loss of −23.95 dB at 8.68 GHz with a thickness of 3 mm and a through power of 99.59%. The incorporation of GNPs can enhance microwave absorption through electrical and dielectric loss mechanisms, contributing to the dissipation of electromagnetic energy as heat [39]. CRH exhibited the best reflection loss of −24.75 dB at 8.84 GHz with a thickness of 3 mm and a through power of 99.66%. The porous carbon structure of CRH is reported to enhance interfacial polarization and dipole relaxation, thereby contributing to electromagnetic wave absorption [40]. Overall, all three single-component materials showed comparable absorption performance, with reflection loss values ranging from −23 to −25 dB.

As shown in **Fig. 10(d)** and **Table 4**, the combination of the three components into the Fe_3O_4/GNPs/CRH nanocomposite led to a marked enhancement in absorption performance relative to the single-component materials. The highest recorded reflection loss was −31.88 dB at 8.6 GHz, corresponding to a thickness of 3 mm and a through power of 99.93%. This enhancement is likely attributable to the combined contribution of magnetic loss originating from Fe_3O_4, conductive loss from GNPs, and interfacial polarization from CRH. Although no instrumental measurement (e.g.directly

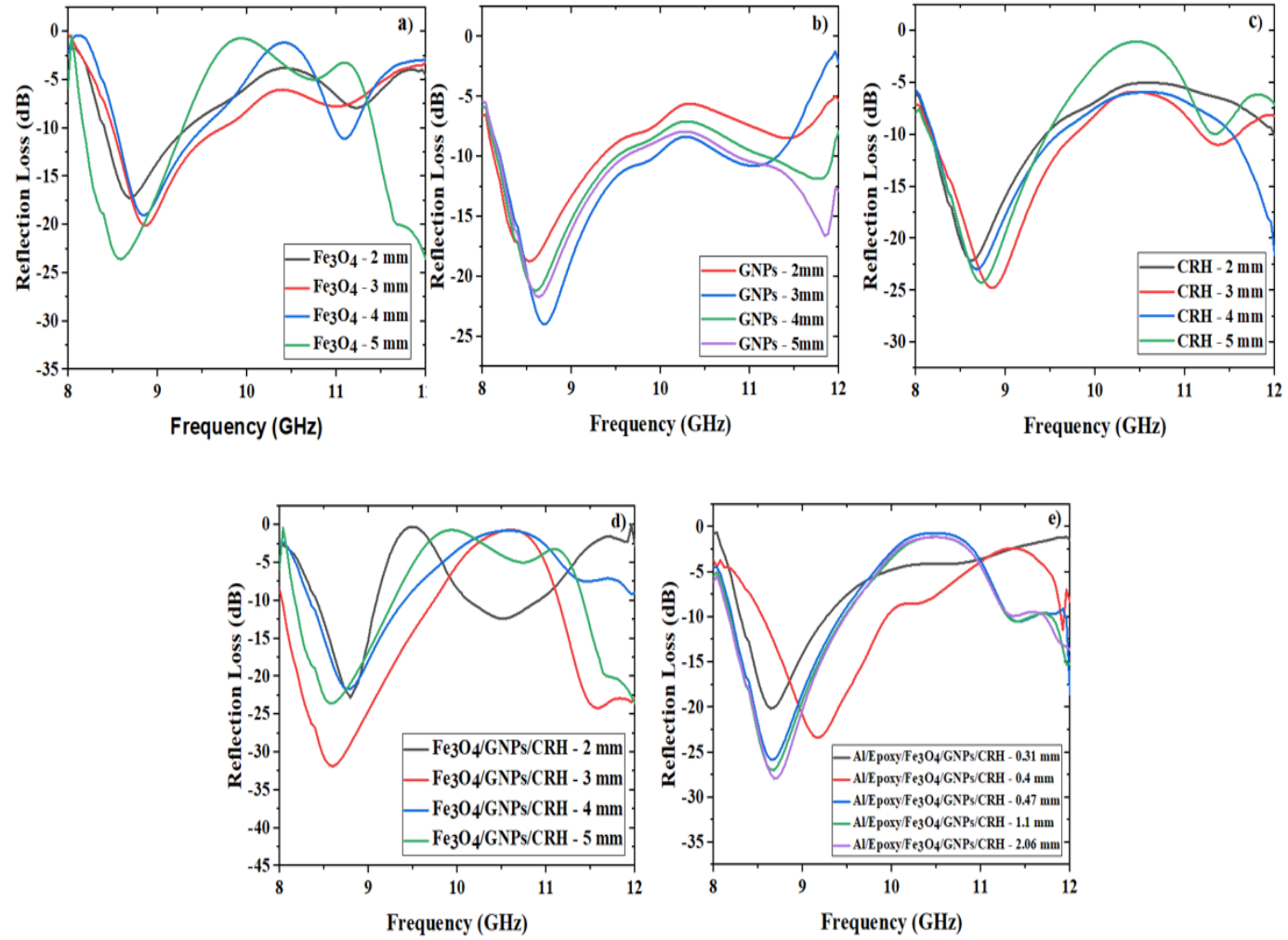


Fig.10 VNA results of (a) Fe_3O_4, (b) GNPs, (c) CRH, (d) Fe_3O_4/GNPs/CRH nanocomposite, and (e) Al/Epoxy/Fe_3O_4/GNPs/CRH coating at various thicknesses within the 8–12 GHz X-band frequency range

quantify the magnetic loss contribution), this interpretation is consistent with mechanisms reported in composites [41-42]. The combination of these contributions may facilitate electromagnetic wave absorption, potentially through improved impedance matching. However, no quantitative impedance-matching calculation (e.g., Z_{in}/Z_0) was performed in this study. Therefore, the role of impedance matching is discussed qualitatively based on the observed RL enhancement and relevant literature [43].

As shown in **Fig. 10(e)** and **Table 4**, the Al/Epoxy/Fe_3O_4/GNPs/CRH coating exhibited RL values that progressively increased with increasing coating thickness. The RL values were −20.15 dB, −23.39 dB, −25.83 dB, −26.98 dB, and −27.92 dB for thicknesses of 0.31 mm, 0.4 mm, 0.47 mm, 1.1 mm, and 2.06 mm, respectively. The highest reflection loss was recorded at a thickness of 2.06 mm, reaching −27.92 dB at 8.68 GHz, with a through power reaching 99.83%. Increasing coating thickness lengthens the propagation path of electromagnetic waves within the material, resulting in more intense interaction between the waves and the absorbing material. It is noted that the RL value obtained for the coating (−27.92 dB) is higher than that of the Fe_3O_4/GNPs/CRH powder composite alone (−31.88 dB). This reduction is reasonably attributed to the dilution effect of the epoxy matrix, which lowers the effective filler loading and disrupts particle-to-particle contact compared with the powder form. Nevertheless, since practical radar-absorption applications require the material to be applied as a durable, substrate-adherent coating rather than as loose powder, the Al/Epoxy/Fe_3O_4/GNPs/CRH coating remains of interest as a candidate radar-absorbing coating, provided further optimization of filler loading and dispersion is carried out to narrow the performance gap with the powder form.

Table 4. Reflection loss and through power of powder and coating materials

Materials	Thickness (mm)	Frequency (GHz)	Reflection Loss (dB)	Through Power (%)
Fe_3O_4	2	8.68	-17.21	98.09
	3	8.88	-20.08	99.01
	4	8.84	-19.04	98.75
	5	8.60	-23.56	99.55
GNPs	2	8.52	-18.71	98.65
	3	8.68	-23.95	99.59
	4	8.60	-21.18	99.23
	5	8.64	-21.68	99.32
CRH	2	8.64	-22.11	99.38
	3	8.84	-24.75	99.66
	4	8.68	-22.97	99.49
	5	8.72	-24.24	99.62
Fe_3O_4/GNPs/CRH	2	8.8	-22.81	99.47
	3	8.6	-31.88	99.93
	4	8.76	-21.68	99.32
	5	8.6	-23.56	99.55
Al/Epoxy/Fe_3O_4/GNPs/CRH	0.31	8.64	-20.15	99.03
	0.40	9.16	-23.39	99.54
	0.47	8.68	-25.83	99.73
	1.10	8.68	-26.98	99.79
	2.06	8.68	-27.92	99.83

The most favorable microwave absorption performance was demonstrated by the Fe_3O_4/GNPs/CRH nanocomposite, achieving a maximum RL of −31.88 dB at 8.6 GHz with a 3 mm thickness and a through power of 99.93%. As for the Al/Epoxy/Fe_3O_4/GNPs/CRH coating, a maximum reflection loss of −27.92 dB was recorded at 8.68 GHz at a thickness of 2.06 mm, accompanied by a through power of 99.83%. All samples demonstrated reflection loss values lower than −10 dB, a threshold widely regarded in the literature as indicative of effective microwave absorption, corresponding to more than 90% of incident wave energy being absorbed [44]. These results indicate that the Al/Epoxy/Fe_3O_4/GNPs/CRH coating shows potential for X-band radar-absorbing applications, although further optimization of filler content and dispersion is needed to improve its absorption performance compared with the powder composite.

4. CONCLUSION

In this study, the Fe_3O_4/GNPs/CRH nanocomposite was successfully synthesized via in situ co-precipitation and used as an epoxy coating on an aluminum substrate for X-band radar absorption. FTIR analysis supported the presence of characteristic functional groups of Fe_3O_4, GNPs, and CRH in the nanocomposite, with several shifts in the absorption bands observed after composite formation. The coating thickness increased with the number of coating cycles, with average thicknesses of 0.311, 0.403, 0.470, 1.100, and 2.066 mm. Water contact angle measurements showed a decrease from 75.38° for the uncoated aluminum to 59.49°, 56.65°, 53.61°, 52.20°, and 51.43° for samples Al1–Al5, respectively. All surfaces exhibited hydrophilic behavior. Nevertheless, the epoxy matrix still served as a physical barrier, limiting direct contact between water or electrolytes and the aluminum substrate.

In terms of microwave absorption performance, the Fe_3O_4/GNPs/CRH nanocomposite exhibited a maximum *reflection loss* (RL) of −31.88 dB at 8.60 GHz for a 3 mm thickness, corresponding to a *through power* of 99.93%. This value was better than those obtained for the individual Fe_3O_4, GNPs, and CRH components, which exhibited maximum RL values of −23.56, −23.95, and −24.75 dB, respectively. The enhanced performance of the nanocomposite can be attributed to the combined contributions of *magnetic loss*, *conductive loss*, and *interfacial polarization* from the respective components, although these contributions were not directly quantified in this study. For the Al/Epoxy/Fe_3O_4/GNPs/CRH system, increasing the coating thickness improved the absorption performance, as indicated by increasingly negative RL values, with a maximum RL of −27.92 dB at 8.68 GHz for a coating thickness of 2.066 mm and a *through power* of 99.83%. The RL of the coating was lower than that of the powder-form nanocomposite, likely due to the dilution effect of the epoxy matrix, which reduced the effective filler concentration and interparticle contact. Nevertheless,

all tested samples exhibited RL values below −10 dB within the X-band frequency range. These results indicate that the Fe_3O_4/GNPs/CRH nanocomposite in an epoxy matrix on an aluminum substrate has potential for further development as a radar-absorbing material for X-band applications, with optimization of filler content and dispersion required to improve coating performance.

5. AUTHOR'S DECLARATION

5.1. Data Availability

There is no supplementary material associated with this manuscript. The data that support the results of this research can be obtained from the corresponding author (RM) upon reasonable request.

5.2. Acknowledgments

We sincerely thank the Functional Nanocarbon Research Group, National Research and Innovation Agency (BRIN), South Tangerang, for their assistance throughout this work.

5.3. Conflict of Interest

There is no conflict of interest in this research.

5.4. Author Contributions

HIA, AH, MZP, SA, RHM, and RM contributed equally to this study. This research was designed and conducted jointly by all listed authors, who also supervised the characterization process. AH, KHTP, and RM contributed to the revision of the manuscript. All authors have read and approved the final version of this manuscript.

5.5. AI Statement

ChatGPT was utilized to enhance the clarity, grammar, and overall readability of this manuscript. All technical content, data interpretation, and conclusions were solely developed and verified by the authors. The final version of the manuscript was thoroughly reviewed to ensure accuracy, coherence, and alignment with the study's findings.

5.6. Funding Statement

This research received no specific grant from any funding agency in the public, commercial, or non-profit sectors.

5.7. Ethical Clearance

Not applicable.

6. REFERENCES

[1] Yilmaz Atay, H., & İçin, Ö. 2020. Manufacturing radar-absorbing composite materials by using magnetic Co-doped zinc oxide particles synthesized by Sol-Gel. *J. Compos. Mater.* 54(26). 4059–4066. doi: https://doi.org/10.1177/0021998320927754

[2] Kim, S.H., Lee, S.Y., Zhang, Y., Park, S.J., & Gu, J. 2023. Carbon-based radar-absorbing materials toward stealth technologies. *Adv. Sci.* 10(32). 1–22. doi: https://doi.org/10.1002/advs.202303104

[3] Ruiz-Perez, F., López-Estrada, S.M., Tolentino-Hernández, R. V., & Caballero-Briones, F. 2022. Carbon-based radar absorbing materials: A critical review. *J. Sci. Adv. Mater. Devices*. 7(3). 100454. doi: https://doi.org/10.1016/j.jsamd.2022.100454

[4] Mohammed, O.K., Tahir, A.S., & Al-Tumah, W.A.G. 2024. Effect of radar-absorbing materials on radar cross-section reduction of complex targets. *Iraqi J. Appl. Phys.* 20(2 A). 209–214. https://doi.org/10.2025/cmj74137

[5] Qu, S., Wu, G., Fang, J., Zang, D., Xing, H., Wang, L., & Wu, H. 2017. *Dielectric and magnetic loss behavior of nano-oxides. Dalam Spectroscopic Methods for Nanomaterials Characterization (Thomas, S., dkk., Eds.). Elsevier. pp. 259–277*. doi: https://doi.org/10.1016/B978-0-323-46140-5.00011-X

[6] Sun, X., He, J., Li, G., Tang, J., Wang, T., Guo, Y., & Xue, H. 2013. Laminated magnetic graphene with enhanced electromagnetic wave absorption properties. *J. Mater. Chem. C.* 1(4). *765–777*. doi: https://doi.org/10.1039/C2TC00159D

[7] Collado, I., Jiménez-Suárez, A., Vázquez-López, A., del Rosario, G., & Prolongo, S.G. 2024. Ultrasonication influence on the morphological characteristics of graphene nanoplatelet nanocomposites and their electrical and electromagnetic interference shielding behavior. *Polymers (Basel)*. 16(8).1068. doi: https://doi.org/10.3390/polym16081068

[8] Wang, X., Xing, X., Zhu, H., Li, J., & Liu, T. 2023. State of the art and prospects of Fe_3O_4/carbon microwave absorbing composites from the dimension and structure perspective. *Adv. Colloid Interface Sci.* 318. 102960. doi: https://doi.org/10.1016/j.cis.2023.102960

[9] Zhang, W., Zheng, Y., Zhang, X., Zhu, Q., Tian, L., Wu, H., Yan, H., & Qi, S. 2019. Structure-microwave absorption performance correlations of GNPs/ZnO nanocomposite absorber: Synthesis, characterization, and mechanism investigation. *Ceram. Int.* 45(10). 13376–13384. doi: https://doi.org/10.1016/j.ceramint.2019.04.033.

[10] Amalia, G.R., Hardiansyah, A., Rasendriya, A.B., Rahmadtullah, I., Setiono, A., & Murniati, R. 2025. Synthesis and characterization of titanium dioxide/graphene nanoplatelets nanocomposites via planetary ball milling for military radar absorbing materials. *Indones. J. Chem. Stud.* 4(1). 22–27. doi: https://doi.org/10.55749/ijcs.v4i1.67

[11] Yavuz, C.T., Mayo, J.T., Yu, W.W., Prakash, A., Falkner, J.C., Yean, S., Cong, L., Shipley, H.J., Kan, A., Tomson, M. and Natelson, D. 2006. Low-field magnetic separation of monodisperse Fe3O4 nanocrystals. *Science.* 314(5801). 964–967. doi: https://doi.org/10.1126/SCIENCE.1131475

[12] Li, B., Weng, X., Sun, X., Zhang, Y., Lv, X., & Gu, G. 2018. Facile synthesis of Fe_3O_4/reduced graphene oxide/polyvinyl pyrrolidone ternary composites and their enhanced microwave absorbing properties. *J. Saudi Chem. Soc.* 22(8). 979–984. doi: https://doi.org/10.1016/j.jscs.2018.02.006

[13] Li, C.Q., Xu, W., Ding, R.C., Shen, X., Chen, Z., Li, M.D., & Wang, G.S. 2019. Tunable High-Performance Microwave Absorption and Shielding by Three Constituent Phases Between rGO and Fe_3O_4@SiO_2 Nanochains. *Front. Chem.* 7(November). 1–9. doi: https://doi.org/10.3389/fchem.2019.00711

[14] He, Y., Hao, S., Chen, Y., Shi, S., Tian, J., & Yang, C. 2025. Biomass-derived porous carbon-based composites for electromagnetic wave absorption. *Adv. Nanocomposites*. 2(August). 162–184. doi: https://doi.org/10.1016/j.adna.2025.08.002

[15] Fang, J., Shang, Y., Chen, Z., Wei, W., Hu, Y., Yue, X., & Jiang, Z. 2017. Rice husk-based hierarchically porous carbon and magnetic particle composites for highly efficient electromagnetic wave attenuation. *J. Mater. Chem. C*. 5(19). 4695–4705. doi: https://doi.org/10.1039/C7TC00987A

[16] Yahaya, N.Z., Salim, S.R., Mustafa, I.S., Razak, N.N.A., & Zahid, L. 2018. Effects of grain sizes on rice husk ash composite as microwave absorber. *J. Phys. Conf. Ser.* 1083(1).012051. doi: https://doi.org/10.1088/1742-6596/1083/1/012051

[17] Melvin, G.J.H., Wang, Z., & Ni, Q.Q. 2019. Electromagnetic wave absorption performance of carbonized rice husk obtained at various temperatures. *Glob. Challenges*. 3(11). 1–5. doi: https://doi.org/10.1002/gch2.201900045

[18] Jin, Y., Yu, H., Wang, Y., Wang, L., & Nan, B. 2024. Recent progress in electromagnetic wave absorption coatings: from

design principles to applications. *Coatings*. 14(5). 607 doi: https://doi.org/10.3390/coatings14050607
[19] Zhu, L., Li, N., & Childs, P.R.N. 2018. Light-weighting in aerospace component and system design. *Propuls. Power Res.* 7(2). 103–119. doi: https://doi.org/10.1016/j.jppr.2018.04.001
[20] Richter, R., Vagias, I., Sani-Taiariol, T., Gomes, N.A.S., Bacci, D., & Baldan, M.R. 2025. Adaptive RF stealth for next-generation long-range cruise missiles through interdisciplinary integration of MnZn ferrite/epoxy RAM and sea-surface multipath null exploitation. *Def. Technol.* 59. 149-165. doi: https://doi.org/10.1016/j.dt.2025.11.010
[21] Barik, R., Pradhan, M., Mahapatra, A., & Nath, G. 2026. Graphene nanoplatelet-reinforced luffa cylindrica fiber/epoxy composites for X-band microwave absorption. *Compos. Commun.* 61. 102682. doi: https://doi.org/10.1016/j.coco.2025.102682
[22] Barik, R. & Nath, G. 2026. Graphene nanoplatelet/α-Fe_2O_3 integrated carbon fiber-based composites for electromagnetic interference shielding and microwave absorption. *Mater. Sci. Semicond. Process.* 202. 110157. doi: https://doi.org/10.1016/j.mssp.2025.110157
[23] Negi, P. & Kumar, A. 2022. Biomass-Derived Activated Carbon/Epoxy Composite as Microwave Absorbing Material. *J. Electron. Mater.* 51(6). 2918–2925. doi: https://doi.org/10.1007/s11664-022-09558-y
[24] Chitraningrum, N., Marlina, R., Arundina, R.Y., Suryani Togatorop, E.R., Sulistyaningsih, Arisesa, H., Budiman, I., Daud, P., & Hamzah, M. 2022. Microwave absorption properties of porous activated carbon-based palm oil empty fruit bunch. *AIP Adv.* 12(11). 35083–35093. doi: https://doi.org/10.1063/5.0128960
[25] Cheng, Y.L., Dai, J.M., Zhu, X.B., Wu, D.J., Yang, Z.R., & Sun, Y.P. 2009. Enhanced microwave absorption properties of intrinsically core/shell structured La 0.6Sr 0.4 nanoparticles. *Nanoscale Res. Lett.* 4(10). 1153–1158. doi: http://dx.doi.org/10.1007/s11671-009-9374-y
[26] Mesa, S., Castro-Ladino, J.R., Amaya, S.L., Manrique, C., Echavarría, A., Hoyos-Ayala, D.A., & Uran, L. 2025. Comprehensive Characterization of Carbonaceous Material Derived from Rice Husk Pyrolysis and Its Potential for CO2 Adsorption. *Materials (Basel).* 18(22). 1–16. doi: https://doi.org/10.3390/ma18225151
[27] Yang, X., Zhou, T., Ren, B., Shi, Z., & Hursthouse, A. 2017. Synthesis, Characterization, and Adsorptive Properties of Fe_3O_4/GO Nanocomposites for Antimony Removal. *J. Anal. Methods Chem.* 2017. 3012364. doi: https://doi.org/10.1155/2017/3012364
[28] Prato, R.A., Van Vught, V., Eggermont, S., Pozo, G., Marin, P., Fransaer, J., & Dominguez-Benetton, X. 2019. Gas Diffusion Electrodes on the Electrosynthesis of Controllable Iron Oxide Nanoparticles. *Sci. Rep.* 9(1). 1–11. doi: https://doi.org/10.1038/s41598-019-51185-x
[29] Wang, F. & Drzal, L.T. 2018. Development of stiff, tough and conductive composites by the addition of graphene nanoplatelets to polyethersulfone/epoxy composites. *Materials (Basel).* 11(11). 2137. doi: https://doi.org/10.3390/ma11112137
[30] Daffalla, S.B., Mukhtar, H., & Shaharun, M.S. 2020. Preparation and characterization of rice husk adsorbents for phenol removal from aqueous systems. *PLoS One*. 15(12). e0243540.doi: https://doi.org/10.1371/journal.pone.0243540
[31] Bakdash, R.S., Aljundi, I.H., Basheer, C., & Abdulazeez, I. 2020. Rice husk-derived aminated silica for the efficient adsorption of different gases. *Sci. Rep.* 10(1). 1–12. doi: https://doi.org/10.1038/s41598-020-76460-0
[32] Akerboom, S., Kamperman, M., & Leermakers, F.A.M. 2016. Three-gradient regular solution model for simple liquids wetting complex surface topologies. *Beilstein J. Nanotechnol.* 7(1). 1377–1396. doi: https://doi.org/10.3762/bjnano.7.129
[33] Li, Y., Wang, G., Guo, Y., Fang, N., Li, J., Li, Z., & Li, J. 2024. Preparation of cardanol-based curing agent for underwater drainage pipeline repairs. *E-Polymers*. 24(1). 20230190.doi: https://doi.org/10.1515/epoly-2023-0190
[34] Alam, K., Jo, Y.Y., Park, C.K., & Cho, H. 2020. Synthesis of graphene oxide using atmospheric plasma for prospective biological applications. *Int. J. Nanomedicine*. 15. 5813–5824. doi: https://doi.org/10.2147/IJN.S254860
[35] Abakah, R.R., Huang, F., Hu, Q., Wang, Y., & Jing, L. 2021. Comparative study of corrosion properties of different graphene nanoplate/epoxy composite coatings for enhanced surface barrier protection. *Coatings*. 11(3). 1–18. doi: https://doi.org/10.3390/coatings11030285
[36] Ji, W.G., Hu, J.M., Liu, L., Zhang, J.Q., & Cao, C.N. 2006. Water uptake of epoxy coatings modified with γ-APS silane monomer. *Prog. Org. Coatings*. 57(4). 439–443. doi: https://doi.org/10.1016/j.porgcoat.2006.09.025
[37] Dandan Doganci, M. & Sevinç, H. 2023. Investigation of superhydrophobic and anticorrosive epoxy films with al2o3 nanoparticles on different surfaces. *ACS Omega*. 8(24). 21559–21570. doi: https://doi.org/10.1021/acsomega.3c00729
[38] Elmahaishi, M.F., Azis, R.S., Ismail, I., Abbas, Z., Matori, K.A., Muhammad, F.D., Saat, N.K., Nazlan, R., Ibrahim, I.R., Abdullah, N.H., & Mokhtar, N. 2021. Structural, electromagnetic and microwave properties of magnetite extracted from mill scale waste via conventional ball milling and mechanical alloying techniques. *Materials (Basel).* 14(22). 7075. doi: https://doi.org/10.3390/ma14227075
[39] Dua, M., Zhang, Q., & Mertiny, P. 2023. Microwave heating of graphene nanoplatelet polymer composites: Experimental and finite element study. *Polym. Compos.* 44(8). 4924–4936. doi: https://doi.org/10.1002/pc.27460
[40] Yan, L., Li, Y., Tong, S., Zhang, K., & Xiang, J. 2024. Controllable surface functionalization of rice husk-derived porous carbon by atomic layer deposition for highly-efficient microwave absorption. *Vacuum*. 224. 113199. doi: https://doi.org/10.1016/j.vacuum.2024.113199
[41] Shi, Y., Yin, Y., Zhang, Y., Hu, Y., & Liu, W. 2019. Preparation and Microwave Absorption Properties of C@Fe_3O_4 Magnetic Composite Microspheres. *Materials.* 12(15). 2404. doi: https://doi.org/10.3390/ma12152404
[42] Kavoosi, V. & Masoudpanah, S.M. 2025. PVP-assisted MOF-derived Fe3O4/C powders for microwave absorption applications. *Heliyon*. 11(1). e41202. doi: https://doi.org/10.1016/j.heliyon.2024.e41202
[43] Xiang, Z., Song, Y., Xiong, J., Pan, Z., Wang, X., Liu, L., Liu, R., Yang, H., & Lu, W. 2019. Enhanced electromagnetic wave absorption of nanoporous Fe3O4 @ carbon composites derived from metal-organic frameworks. *Carbon N. Y.* 142. 20–31. doi: https://doi.org/10.1016/j.carbon.2018.10.014
[44] Gao, S., An, Q., Xiao, Z., Zhai, S., & Shi, Z. 2018. Significant promotion of porous architecture and magnetic Fe3O4 NPs inside honeycomb-like carbonaceous composites for enhanced microwave absorption. *RSC Adv.* 8(34). 19011–19023. doi: https://doi.org/10.1039/c8ra00913a